Rational Design of Photoconvertible and Biphotochromic Fluorescent Proteins for Advanced Microscopy Applications

Virgile Adam, Benjamien Moeyaert, Charlotte c. David, Hideaki Mizuno, Mickaël Lelimousin, Peter Dedecker, Ryoko Ando, Atsushi Miyawaki, Jan Michiels, Yves Engelborghs, et al.

Chemistry & Biology
Article

Rational Design of Photoconvertible and Biphotochromic Fluorescent Proteins for Advanced Microscopy Applications

Virgile Adam,[1,6,7,*] Benjamien Moeyaert,[1,6] Charlotte C. David,[1] Hideaki Mizuno,[1] Mickaël Lelimousin,[4] Peter Dedecker,[1] Ryoko Ando,[5] Atsushi Miyawaki,[5] Jan Michiels,[3] Yves Engelborghs,[2] and Johan Hofkens[1]
[1]Laboratory of Photochemistry and Spectroscopy, Department of Chemistry
[2]Laboratory of Biomolecular Dynamics, Department of Chemistry
[3]Centre of Microbial and Plant Genetics, Department of Microbial and Molecular Systems
Katholieke Universiteit Leuven, 3001 Heverlee, Belgium
[4]Department of Biochemistry, University of Oxford, Oxford OX1 3QU, UK
[5]Laboratory for Cell Function Dynamics, RIKEN Brain Science Institute, Wako-city, Saitama, 351-0198, Japan
[6]These authors contributed equally to this work
[7]Present address: Pixel Team, IBS, Institut de Biologie Structurale Jean-Pierre Ebel, CEA, CNRS, Université Joseph Fourier, 41 rue Jules Horowitz, F-38027 Grenoble, France and Institut de Recherches en Technologies et Sciences pour le Vivant, iRTSV, Laboratoire de Physiologie Cellulaire et Végétale, CNRS/CEA/INRA/UJF, Grenoble, 38054, France
*Correspondence: virgile.adam@ibs.fr
DOI 10.1016/j.chembiol.2011.08.007

SUMMARY

Advanced fluorescence imaging, including subdiffraction microscopy, relies on fluorophores with controllable emission properties. Chief among these fluorophores are the photoactivatable fluorescent proteins capable of reversible on/off photoswitching or irreversible green-to-red photoconversion. IrisFP was recently reported as the first fluorescent protein combining these two types of phototransformations. The introduction of this protein resulted in new applications such as super-resolution pulse-chase imaging. However, the spectroscopic properties of IrisFP are far from being optimal and its tetrameric organization complicates its use as a fusion tag. Here, we demonstrate how four-state optical highlighting can be rationally introduced into photoconvertible fluorescent proteins and develop and characterize a new set of such enhanced optical highlighters derived from mEosFP and Dendra2. We present in particular NijiFP, a promising new fluorescent protein with photoconvertible and biphotochromic properties that make it ideal for advanced fluorescence-based imaging applications.

INTRODUCTION

Recently developed imaging methodologies such as photoactivated localization microscopy (PALM), stochastical optical reconstruction microscopy (STORM), and derived techniques, have revolutionized fluorescence microscopy by improving the spatial resolution beyond the diffraction limit of light (Betzig et al., 2006; Dedecker et al., 2007; Flors et al., 2007; Heilemann et al., 2008; Hell, 2007; Hess et al., 2006; Rust et al., 2006). All of these approaches make use of the dynamic nature of fluorescence emission at the single-molecule level, and some of the most promising techniques make use of fluorophores that can be controllably converted from a detectable to a nondetectable state or vice versa (Habuchi et al., 2005; Heilemann et al., 2009).

In biological samples, the use of photoactivatable fluorescent proteins (PAFPs) has the advantage of allowing genetically-encoded labeling of a target protein. This can be implemented in a specific and noninvasive fashion for diffraction-unlimited fluorescence microscopy with a fluorophore that can change its optical properties on demand. However, the use of PAFPs has several drawbacks such as their limited number of emitted photons during one switching event compared to synthetic dyes, and the fact that their complex photophysics remain only partially understood. At present three different classes of these labels have been identified, involving reversible on/off switching of the fluorescence, irreversible green-to-red conversion, and irreversible off-to-on fluorescence conversion (Lukyanov et al., 2005).

Recently, a new fluorescent protein, IrisFP, was reported (Adam et al., 2008). This PAFP combines both irreversible green-to-red photoconversion upon intense irradiation with 405-nm light and reversible on/off switchings in both the green and red forms. Wavelengths for on/off photoswitchings in green and red forms are 405/488 nm and 440/561 nm, respectively. Very low 405-nm light intensity is required to perform the highly efficient off-to-on switching of the green form compared to the green-to-red photoconversion. Not only could such protein be used for quaternary data storage (Adam et al., 2010), the irreversible conversion from green to red allows two subpopulations of the same protein to be distinguished, whereas the reversible photoswitching allows subdiffraction imaging of both states, opening up the possibility of pulse-chase super-resolution imaging (Fuchs et al., 2010). Practical applications, however, remain limited by the rather fast off-switching rate and low photostability of IrisFP, drastically restricting the number

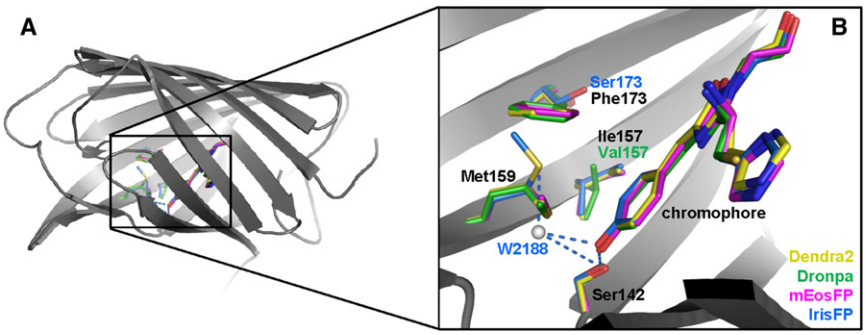

Figure 1. Localization of Amino Acids Influencing the Photoisomerization of the Chromophore

(A) Typical β-barrel folding of fluorescent proteins. (B) Superposition of the chromophore and surrounding residues in the green forms of Dendra2 (yellow, PDB: 2VZX), Dronpa (green, PDB: 2Z1O), mEosFP (pink, PDB: 3P8U), and IrisFP (blue, PDB: 2VVH). Residues 142, 157, 159, and 173 are represented; residues differing from the consensus amino acid are labeled in the color corresponding to the protein. The white sphere represents the water molecule that interacts with Ser142 in IrisFP (specific hydrogen bonds in IrisFP represented in blue dashes). See also Figure S1 and Table S1.

of photons that can be extracted from a single switching event. In addition, its validity as a fusion partner in biological samples is limited by its oligomeric nature. Although a monomeric variant (mIrisFP) has been reported (Fuchs et al., 2010), it does not fully address the above-mentioned spectroscopic limitations; e.g., mIrisFP is still only moderately photoconvertible to the red state (see Table S1 available online). All these parameters complicate the use of (m)IrisFP in advanced fluorescence imaging.

The investigation of the chromophore interaction with its environment inside the β-barrel structure led to the improvement of spectral properties in many (PA)FPs (Adam et al., 2008, 2009; Andresen et al., 2007; Hayashi et al., 2007; Henderson et al., 2007; Nienhaus et al., 2006; Subach et al., 2009, 2010; Tsutsui et al., 2009). These experimental studies have been supported by molecular and quantum mechanics calculations (Lelimousin et al., 2009a; Li et al., 2010; Moors et al., 2008; Voliani et al., 2008) and spectroscopic studies (Abbruzzetti et al., 2010; Dedecker et al., 2006; Habuchi et al., 2006; Hendrix et al., 2008; Mizuno et al., 2008) that has improved our understanding about the complex photophysics of these molecules.

In this study, we describe a number of structural themes of major importance for the introduction of on/off photochromism in virtually any green-to-red photoconvertible fluorescent protein (PCFP). Recent publications (Adam et al., 2008; Andresen et al., 2008; Bizzarri et al., 2010; Moors et al., 2008; Piatkevich and Verkhusha, 2010; Subach et al., 2009, 2010; Tsutsui et al., 2005; Voliani et al., 2008) have shown that the reversible photoswitching and irreversible photoconversion of fluorescent proteins are largely controlled by a few key residues surrounding the chromophore. In the case of PAFPs, the residues at positions 157, 159, and 173 (numbering in accordance with IrisFP, corresponding to residues 165, 167, and 181 in EGFP) (Figure 1; Figure S1, and Table S1) are well conserved in terms of identity and conformation in all green-to-red PCFPs known to date. We hypothesized that by making selected mutations at these positions in PCFPs with favorable properties, it should be possible to rationally engineer a new range of better performing four-way optical highlighters. Here we demonstrate that by combining prior knowledge of the structure of fluorescent proteins and our understanding of the relation between the structure and the corresponding photophysical and photochemical properties we can rationally design molecules with improved characteristics for advanced imaging applications such as super-resolution microscopy, time-lapse microscopy, pulse-chase imaging, or single-particle tracking.

RESULTS AND DISCUSSION

When discussing the photophysics of reversibly switchable fluorescent proteins (RSFPs), the residues at position 157, 159, and 173, located around the chromophore, are of major importance (Figure 1; Figure S1). Mutating one or more of these residues generally affects the photochromic behavior (Table S1) as was demonstrated in Dronpa (Ando et al., 2004) variants such as rsFastLime (V157G) (Stiel et al., 2007), bsDronpa (V157G/M159C/F173C) (Andresen et al., 2008), Padron (V157G/M159Y) (Andresen et al., 2008), Dronpa-2 (M159T) (Ando et al., 2007), or Dronpa-3 (V157I/M159A) (Ando et al., 2007). Another example is IrisFP (Adam et al., 2008), where photochromic behavior was introduced into the green-to-red PCFP EosFP thanks to one targeted mutation (EosFP F173S) whose influence is well understood thanks to the crystal structures of both proteins. These findings are particularly remarkable when one considers the high degree of structural similarity in the position and conformation of the chromophore and the above-mentioned amino acids (Figure 1). On this basis, we reasoned that introducing on/off switching properties like that of EosFP/IrisFP might be possible in all PCFPs.

Mutating Phe173 to Ser results in a flip of the Met residue at position 159 toward the Ser173. This allows for a water molecule (W2188 in IrisFP; Figure 1) to enter the barrel and interact with Ser142. This change in the environment of the chromophore enables the *cis-trans* isomerization that is coupled with on/off photochromism for most RSFPs. As the environment of the chromophore is so similar in all PCFPs, we reasoned that mutating the well-conserved Phe173 to Ser in any green-to-red PCFP might induce on/off photochromism.

As the effect on on/off photochromism of the F173S mutation has been reported as indirect, we reasoned that mutating the residue Met159 might induce a more direct effect and could result in interesting properties in terms of on- or off-switching. Thus, as a second targeted mutation, Met159 was substituted with a small aliphatic amino acid (Ala), with which we hoped to introduce on/off photochromic properties to any green-to-red PCFP. The residue has to be small, to allow conformational freedom for *cis-trans* isomerization of the chromophore, as

Table 1. Photophysical Properties of All Proteins and Mutants Presented in This Study

		mEosFP	mEosFP M159A	mEosFP F173S	Dendra2	Dendra2 M159A	Dendra2 F173S	Dronpa	IrisFP	mIrisFP
Green species	λ_{ex} (nm)	504	487	486	490	471	469	503	488	486
	λ_{em} (nm)	516	512	514	505	504	507	517	516	516
	Stokes shift (nm)	12	25	28	15	33	38	14	28	30
	pKa	5.3 [5.5]	4.3	5.8	7.2 [7.1]	6.5	7.0	5.3 [5.0]	5.7 [6.4]	5.7 [5.4]
	ε ($M^{-1} \times cm^{-1}$)	97,200 [67,200]	98,600	53,200	45,100 [45,000]	51,100	41,100	94,100 [95,000]	57,800 [52,000]	74,000 [47,000]
	Φ_{fluo}	0.67	0.52	0.43	0.55 [0.50]	0.55	0.64	0.67 [0.85]	0.48 [0.43]	0.60 [0.54]
	Brightness	1.94	1.53	0.68	0.74	0.84	0.78	1.88	0.83	1.32
	Φ_{off}	1.8×10^{-7}	2.6×10^{-3}	2.2×10^{-3}	5.7×10^{-6}	1.1×10^{-3}	1.8×10^{-3}	3.0×10^{-4}	3.2×10^{-3}	2.2×10^{-3}
	Φ_{on}	0.79	0.15	0.20	0.10	0.08	0.10	0.70	0.15	0.13
Red species	λ_{ex} (nm)	569	NA	550	553	528	526	NA	551	546
	λ_{em} (nm)	581	NA	581	573	562	569	NA	580	578
	Stokes shift (nm)	12	NA	31	20	34	43	NA	29	32
	pKa	6.5 [5.5]	NA	6.2	7.8 [7.5]	6.8	7.3	NA	6.8 [7.2]	7.0 [7.6]
	ε ($M^{-1} \times cm^{-1}$)	41,300 [37,000]	NA	25,000	36,200 [35,000]	45,000	42,000	NA	27,000 [35,000]	26,000 [33,000]
	Φ_{fluo}	0.66	NA	0.41	0.55 [0.55]	0.75	0.65	NA	0.50 [0.47]	0.44 [0.59]
	Brightness	0.81	NA	0.31	0.55	1.00	0.81	NA	0.40	0.34
	Φ_{off}	3.5×10^{-5}	NA	0.4×10^{-3}	5.0×10^{-7}	3.2×10^{-3}	1.0×10^{-3}	NA	2.0×10^{-3} [2.0×10^{-3}]	0.4×10^{-3} [0.3×10^{-3}]
	Φ_{on}	0.05	NA	0.06	0.50	0.01	0.10	NA	0.05 [0.047]	0.11 [0.28]

Brightness is expressed relative to EGFP. Values previously reported in different literature sources are shown between brackets and are extracted from Wiedenmann et al. (2004) (mEosFP), Gurskaya et al. (2006), Adam et al. (2009), Hoi et al. (2010) (Dendra2), Ando et al. (2004) (Dronpa), Adam et al. (2008) (IrisFP), and Fuchs et al. (2010) (mIrisFP). NA, not applicable.

well as to allow increased flexibility of the whole chromophore environment. An aliphatic residue was chosen in order to avoid unpredictable side-effects coming from H-bond interactions involving this new residue. Of course, the combination of both mutations might be interesting. In such double mutant, Phe173 could for instance be mutated not to the polar Ser, but rather to an aliphatic residue like Leu. We hypothesized that this mutation will reduce polar interactions that stabilize the off state.

As a third target, we looked at the residue at position 157. In PCFPs, this residue is Ile or Val. In Dronpa and its mutants, it regulates the proteins' switching speed (Table S1), and in IrisFP it was shown to change orientation between the *cis*- and *trans*-conformation. Mutating the residue at this position to Ala, that is aliphatic like Leu or Val, but is much smaller, is a possible third route to inducing reversible photoswitching in PCFPs by introducing structural flexibility.

To test whether the three targeted mutations introduce the expected behavior, we chose to imply these three mutation strategies, one at a time, on Dendra2. Dendra2 is a green-to-red PCFP that exhibits the favorable properties of being monomeric, having a high brightness and an efficient photoconversion (Adam et al., 2009; Chudakov et al., 2007; Gurskaya et al., 2006). We thus hoped to create a four-way highlighter probe that is better performing in advanced microscopy applications.

We also constructed mEosFP M159A and mEosFP F173S from mEosFP A69V, a monomeric variant of EosFP (kindly provided by U. Nienhaus). For clarity, we refer to mEosFP A69V as mEosFP throughout this article.

Spectroscopic Characterization of Photoactivation Behavior

We characterized the spectroscopic behavior of the ancestors and engineered mutants in detail (Table 1; Figure S2). All mutants were fluorescent, and all but Dendra2 I157A displayed the expected multiphotoactivatable behavior. Dendra2 I157A is efficiently green-to-red photoconvertible, but is essentially non-photochromic (data not shown); its behavior was not remarkably different from Dendra2. This indicates that this single mutation is not sufficient to induce photochromism on its own, although it can alter the photochromic behavior in certain fluorescent proteins.

Dendra2 M159A/F173L displayed behavior that was almost identical to that of Dendra2 M159A (vide infra), meaning that both green-to-red photoconversion and on/off photoswitching were present and that quantum yields for on- and off-switching were almost identical for these two proteins (data not shown). Thus, extra conformational freedom of the chromophore as compared to Dendra2 M159A does not seem to result in substantially altered photochromic behavior. The photophysical properties of Dendra2 I157A and Dendra2 M159A/F173L are almost identical to those of Dendra2 and Dendra2 M159A, respectively, and hence, we do not discuss them further.

We observed reversible photoswitching in mEosFP and Dendra2 (Figure S2) even though such reversible photoswitching in these supposedly non-RSFPs has not been previously reported at the ensemble level. A recent publication, however, reports the case of a reversible long-living dark state in single molecules of mEos2, variant of mEosFP, spin-coated in a matrix of polyvinyl-alcohol (Annibale et al., 2010). We measured quantum yields of off-switching of $\sim 10^{-7}$, which is very low and probably the reason that this phenomenon was not identified in these proteins before. The on-switching quantum yield, induced by 405-nm light, ranges from 0.79 for the green form of mEosFP to 0.01 for the red form of Dendra2 M159A, though the reasons for this remarkable difference remain unclear.

All but one of the mutants (mEosFP M159A) retained their green-to-red photoconversion properties. Although Dendra2 and its mutants were easily converted to the red form with 405-nm light, this process was much more difficult with (m)IrisFP, mEosFP and mEosFP F173S. This reflects the less efficient conversion in mEosFP and its mutants compared to Dendra2. Additionally we found that the photoconversion process in mEosFP-based mutants resulted in a clearly visible precipitate in the protein solution (data not shown). This behavior might be due to a reduced solubility of the red species and is likely to complicate the use of mEosFP mutants in advanced imaging applications.

Among the factors contributing to the observed photoconversion, the pKa of the chromophore and its environment is influenced by the mutations we describe. Because the photoconversion process originates from the neutral state of the chromophore, decreasing its stability results in a reduced green-to-red photoconversion efficiency. This same finding has already been applied to explain the difference in conversion efficiency between EosFP and Dendra2, where an electrostatic interaction in EosFP is disrupted in Dendra2 (Adam et al., 2009). This is readily seen from the measured pKa values of the chromophore of each protein (Table 1; Figure S3). The most acidic pKa was found for mEosFP M159A ($\sim$4.3), partially explaining why this mutant is not photoconvertible at pH 7.4. Dendra2 and its mutants show markedly higher pKa values ($\geq$6.5), and are indeed more efficiently photoconvertible at physiological pH. This is explained by high pKa values for Dendra2 (>7.0), as determined in this study and others (Adam et al., 2009; Hoi et al., 2010).

By itself, the electrostatic role of the residues at positions 159 and 173 is not sufficient to fully explain the observed photoconversion behavior, because decreasing the pH does not necessarily result in increased photoconversion efficiency. Other factors thus have an influence on the photochromism or green-to-red photoconversion. Unambiguously determining these factors, however, is an intricate task that is beyond the scope of this study.

Oligomerization Behavior

As was anticipated, Dendra2 and its mutants proved to be more stable as a monomer than mEosFP F173S, as shown in Figure 2. In particular, we notice that IrisFP and mEosFP F173S, as well as Dronpa, which is known to be monomeric (Mizuno et al., 2010a), are forming oligomers in the range of 100–500 μM, which is the typical expression level of actin in motile cells, for example

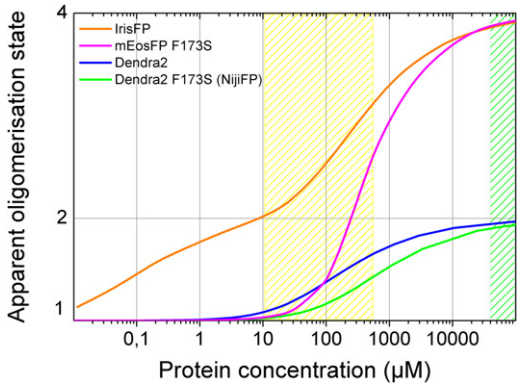

Figure 2. Apparent Oligomerization State of IrisFP, mEosFP F173S, Dendra2, and NijiFP (Dendra2 F173S)

Curves are derived from the association coefficients for dimerization and tetramerization determined by analytical ultracentrifugation. The biological range of protein expression is indicated by yellow shading, the protein concentration in crystals is indicated by green shading. See also Figure S4 and Figure S5.

(Koestler et al., 2009), whereas Dendra2 and Dendra2 F173S remain largely monomeric in this range. This stability of the monomeric form is of crucial importance for a genetic fluorescent reporter regarding the local protein density in cells that can be very high (for example in actin fibers) and regarding cells overexpressing fusion proteins.

Describing the data for IrisFP and mEosFP F173S requires a model involving monomers, dimers, and tetramers, whereas Dendra2 and Dendra2 F173S requires a model consisting of monomers and dimers only (data points could not be fitted with the tetramer model). This is consistent with the oligomerization behavior under very high protein concentration; in crystals (protein concentration > 30 mM), mEosFP forms a tetramer in the asymmetric unit whereas Dendra2 only forms dimers and shows no tetramerization (Figure S4).

The crystal structure of mEosFP (EosFP V123T/T158H) was determined at 2.25-Å resolution (Table S2). This structure clearly shows that interactions at the A/B and A/C interfaces are disrupted as compared to EosFP (Figure S5), leading to a reduced tendency to oligomerize. However, two pairs of His residues, one at each interface, still allow π-stacking, resulting in a tetrameric organization at higher protein concentrations (Figure 2). Among all proteins measured, Dendra2 F173S showed the least tendency to oligomerize at any given concentration.

Modeling of mEosFP and mEosFP M159A

We performed molecular dynamics (MD) simulations based on the X-ray structure of mEosFP that we solved (Protein Data Bank [PDB] ID: 3P8U) in order to better understand the origin of the low pKa of mEosFP. We probed likely structural changes induced by both protonation of the chromophore and mutation M159A in this protein. The results are illustrated in Figure 3, and energies of the molecular interactions involved are summarized in Table S3.

The modeling of the anionic form of mEosFP suggests that Ser142 and a water molecule (W1) stabilize the hydroxybenzylidene moiety of the chromophore by hydrogen bonds (Figure 3A).

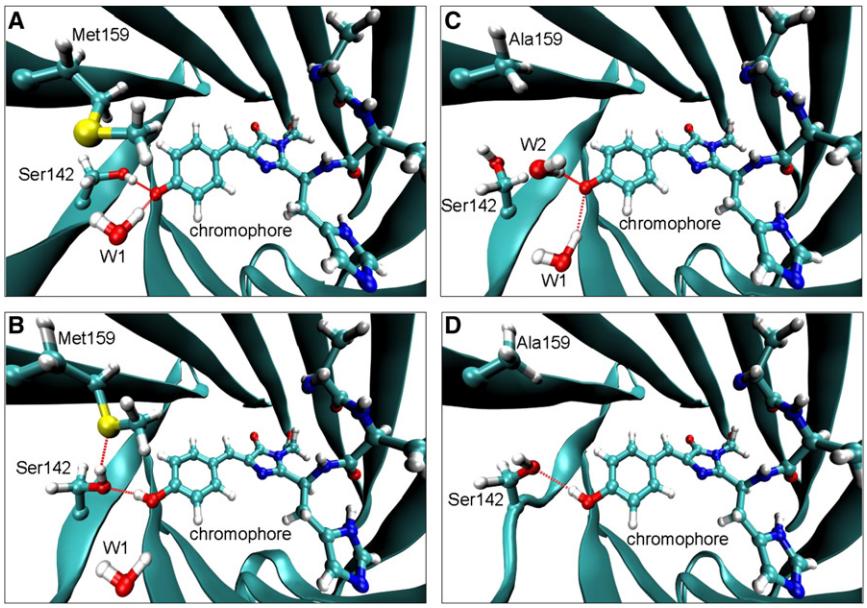

Figure 3. Langevin MD Simulations of mEosFP and mEosFP M159A

(A) Anionic and (B) neutral forms of mEosFP, (C) anionic and (D) neutral forms of mEosFP M159A. Only residues and water molecules of particular interest are represented within the β-barrel structure. Hydrogen bonds between the hydroxyl group of the chromophore and available partners are shown in red dotted lines, whereas hydrogen, carbon, nitrogen, oxygen, and sulfur atoms are drawn in white, cyan, blue, red, and yellow spheres, respectively. See also Table S2 and Table S3.

These interactions are estimated as −30.6 and −45.2 kJ/mol, respectively, whereas Met159 weakly interacts with the chromophore (Table S3). Because we could not obtain crystals at low pH, two distinct models of the neutral form of mEosFP were made, by considering the initial orientation of the hydroxyl group either toward Ser142 or W1. Each simulation quickly converged in the first configuration (Figure 3B). In this state, Met159 is an acceptor of a hydrogen bond shared with Ser142. Met159 also stabilizes the chromophore by both electrostatic and van der Waals interactions with a total energy of −14.4 kJ/mol. The hydrogen bond between the chromophore and W1 is not maintained in the neutral form. In fact, the water molecule diffuses to the bulk solvent during one of the two simulations, which suggests a likely mechanism for the protonation equilibrium of the chromophore. Overall, the model of the anionic form is much closer to the crystal structure than that of the neutral form, which is consistent with the pH of crystallization (pH 8.5).

In the modeling of mEosFP M159A, we chose to include a water molecule (W2) in hydrogen bond interaction with the hydroxyl group of the chromophore, similar to the water molecule observed in the crystal structure of IrisFP (W2188 in Figure 1). Our simulation of the anionic form suggests that W2 contributes along with W1 in stabilizing the phenolate moiety of the chromophore (Figure 3C). These water-chromophore interactions are strong, estimated to be −92.7 kJ/mol and as a result, Ser142 orientates toward the solvent to find another hydrogen bond partner. Similar to mEosFP, two initial orientations were considered for the hydroxyl group of the neutral chromophore in mEosFP M159A. Contrary to the anionic form, both simulations result in a configuration in which the two water molecules W1 and W2 leave into the solvent and Ser142 remains the only hydrogen-bond partner of the phenol ring (Figure 3D).

Overall, the results of molecular modeling provide an explanation for the decrease of pKa induced by the M159A mutation (Table 1; Figure S3). In mEosFP, the main role of Met159 is to stabilize the neutral state of the chromophore and the M159A mutation cancels this stabilization (Table S3). On the other hand, the anionic form may take advantage of the mutation by reorganizing and optimizing the hydrogen bond network surrounding the hydroxylate group of the chromophore. As a consequence, the M159A mutation disfavors photoconversion by lowering the fraction of neutral forms in the sample. An opposite effect has been observed in the structural comparison between EosFP and Dendra2, where an electrostatic interaction in EosFP is disrupted in Dendra2 (Figure S1B). This disruption decreases the stability of the anionic chromophore, resulting in a larger fraction of the neutral form and thus promoting photoconversion (Adam et al., 2009).

Influence of the Chromophore Environment

The decrease of pKa induced by the M159A mutation is consistent with the improved off-switching rate that is activated from the anionic forms. Simulations also show that Met159 stabilizes the presence of Ser142 inside the β-barrel (Figure 3). A previous study already mentioned that this interaction destabilizes the putative *trans* conformation of EosFP by preventing Ser142 finding hydrogen bond partners (Adam et al., 2008). In contrast, the crystal structures of RSFPs in their dark state show Ser142 orientated either inside the β-barrel or within the solvent. Therefore, we believe that releasing the constraint from Met159 may help Ser142 to find a stabilizing environment in the *trans* configuration of mEosFP M159A. The observation that the photoswitching tendency of FPs is strongly determined not only by interactions of amino acids with the chromophore, but also by the opportunity for residues neighboring the chromophore to interact, has already been highlighted in other studies (Mizuno et al., 2008).

The loss of the β strand structure observed in the neutral form of mEosFP M159A at the level of Ser142 provides evidence of substantial flexibility in the protein structure (Figure 3D). This state displays similar features to those observed at room temperature for the dark form of Dronpa, though in that case the chromophore lost its interaction with Ser142 (Mizuno et al., 2008, 2010b).

We determined the fluorescence lifetimes for mEosFP, Dendra2 and their mutants (Table 2). Although the fluorescence

Table 2. Fluorescence Lifetimes of mEosFP, Dendra2, and Their Variants

Proteins		Amplitudes		Lifetimes/ns	
		A_1	A_2	τ_1	τ_2
Green	mEosFP	1	—	3.5	—
	mEosFP F173S	0.6	0.4	3.3	2.3
	mEosFP M159A	0.7	0.3	3.2	2.0
Red	mEosFP	1	—	4.1	—
	mEosFP F173S	0.8	0.2	3.7	1.3
	mEosFP M159A	NA	NA	NA	NA
Green	Dendra2	1	—	3.3	—
	Dendra2 F173S	0.5	0.5	3.4	2.5
	Dendra2 M159A	0.7	0.3	2.8	1.6
Red	Dendra2	1	—	4.4	—
	Dendra2 F173S	0.9	0.1	4.2	1.6
	Dendra2 M159A	1	—	4.0	—

All experimental values exhibit a χ^2 value $\leq$1.1. Excitation wavelengths were 488 nm and 550 nm for green and red samples, respectively. The proteins were diluted in PBS buffer pH 7.4 to ensure a maximal optical density of <0.1. NA, not applicable.

decays of mEosFP and Dendra2 could be fitted using a single-exponential model in both the green and the red state, this was not the case for the mutants, whose decays required fitting with a two-component model. This suggests the existence of multiple conformations in the mutants and hence an increase flexibility of the chromophore. By introducing mutations in the microenvironment of the chromophore, we destabilized its very rigid structure. This results in a less tightly packed and more flexible chromophore that is more prone to collisional quenching and/or other nonradiative decay mechanisms, leading to a decrease in lifetimes (Table 2) (Lelimousin et al., 2009b; Millington et al., 2007; Seifert et al., 2002). Interestingly, the mutations seem to have less effect on the red state than on the green state, which could be explained by a better stabilized chromophore in the red state as evidenced by the longer lifetimes.

Evidence for the increased flexibility of the chromophore of mEosFP mutants as compared to their parent protein also comes from the decrease in fluorescence quantum yield of these mutants (Table 1). This also has been reported for other FPs (Shu et al., 2006). Correspondingly, in MD simulations, we see that the M159A mutation provides more free space in the environment of the chromophore (Figure 3). This observation is also made for IrisFP and its parent EosFP (Adam et al., 2008) as well as for bsDronpa and its parent Dronpa (Andresen et al., 2008). Indeed it has become largely accepted that a higher flexibility of the chromophore might lead to a more efficient photoswitching, but this comes at the cost of a decreased fluorescence quantum yield (Lelimousin et al., 2009b; Stiel et al., 2007).

We also observed a blue shift in the absorption spectra of the mutants (Figure S2). Our modeling experiments suggest a better stabilization of the electron density on the phenolate group of the chromophore of the mutants in the ground state, by hydrogen bonding interactions with the water molecules W1 and W2 (Table S3). This electrostatic stabilization may be nullified during excitation by charge transfer from the phenolate to the imidazole moiety of the chromophore (Voityuk et al., 1998). Consequently, both wild-types and mutants should reach a similar level of energy in the excited state, resulting in different energy gaps with the ground state. Unlike the absorption spectra, the emission maxima remain largely unchanged. The environment of the chromophore in the mutants may enable a more pronounced relaxation of the excited state to show similar emission wavelength as the parent proteins. This results in a larger Stokes shift in the mutants (up to ~40 nm), which is advantageous for microscopic applications in order to easily separate excitation and emission bands.

Advanced Microscopic Imaging Using NijiFP (Dendra2 F173S)

Based on the results and spectroscopic parameters described above, we reasoned that Dendra2 F173S is the most promising of the fluorescent proteins described here for advanced microscopic applications. It is not as bright as some of the other mutants, but is effectively photochromic and displays very efficient photoconversion. We named this protein NijiFP, after the Japanese word for rainbow and as a reference to IrisFP, named after the Greek goddess personifying the rainbow. The pH-dependent change in the protein color is depicted by photographs of solution either in the anionic or neutral form of the chromophore (Figure 4A). Spectra of the green (Figure 4B) and red (Figure 4C) states in both the on- and the off-state are shown. In NijiFP, irreversible photoconversion from the green to the red state is readily observed by irradiating the protein solution with 405-nm light (Figure 4D). It also shows excellent on/off switching properties with a minimal photofatigue in both green state (Figure 4E) and red state (Figure 4F). Decays in intensity after many on/off switchings are well fitted by a stretched exponential function. With the conditions we used (Figure 4), green and red signals decay by 50% in ~150 and ~90 switchings, respectively.

To explore the applications of NijiFP in fluorescence microscopy, we cloned the protein as a fusion construct to actin and expressed these constructs in living HeLa cells. The green emission from labeled actin filaments was readily observed with a confocal microscope and could be efficiently and reversibly switched off and back on. Irradiation with violet light allowed the green fluorescent species to be efficiently converted to the red emitting species within a well-defined region of interest. Both forms could then be reversibly switched on and off with excellent contrast (Figure 5A). Comparison with Dendra2-fused actin in cells, revealed that NijiFP displays a similar photoconversion efficiency, but the red form of NijiFP was more photostable than that of Dendra2 (Figure S6). Similar time-lapse experiments revealed the superior photoconversion properties of NijiFP compared to mEosFP F173S and also clearly demonstrates that the green form of NijiFP and mEosFP F173S can be efficiently switched off with 488-nm light, as compared to mEosFP and Dendra2 (Figure S7).

As a further demonstration of the potential of NijiFP for advanced fluorescence microscopy applications, we subjected the cells expressing NijiFP-fused actin to PALM imaging (Figure 5B) in both the green and the red state. The obtained PALM images can be seen in the middle of the green and red

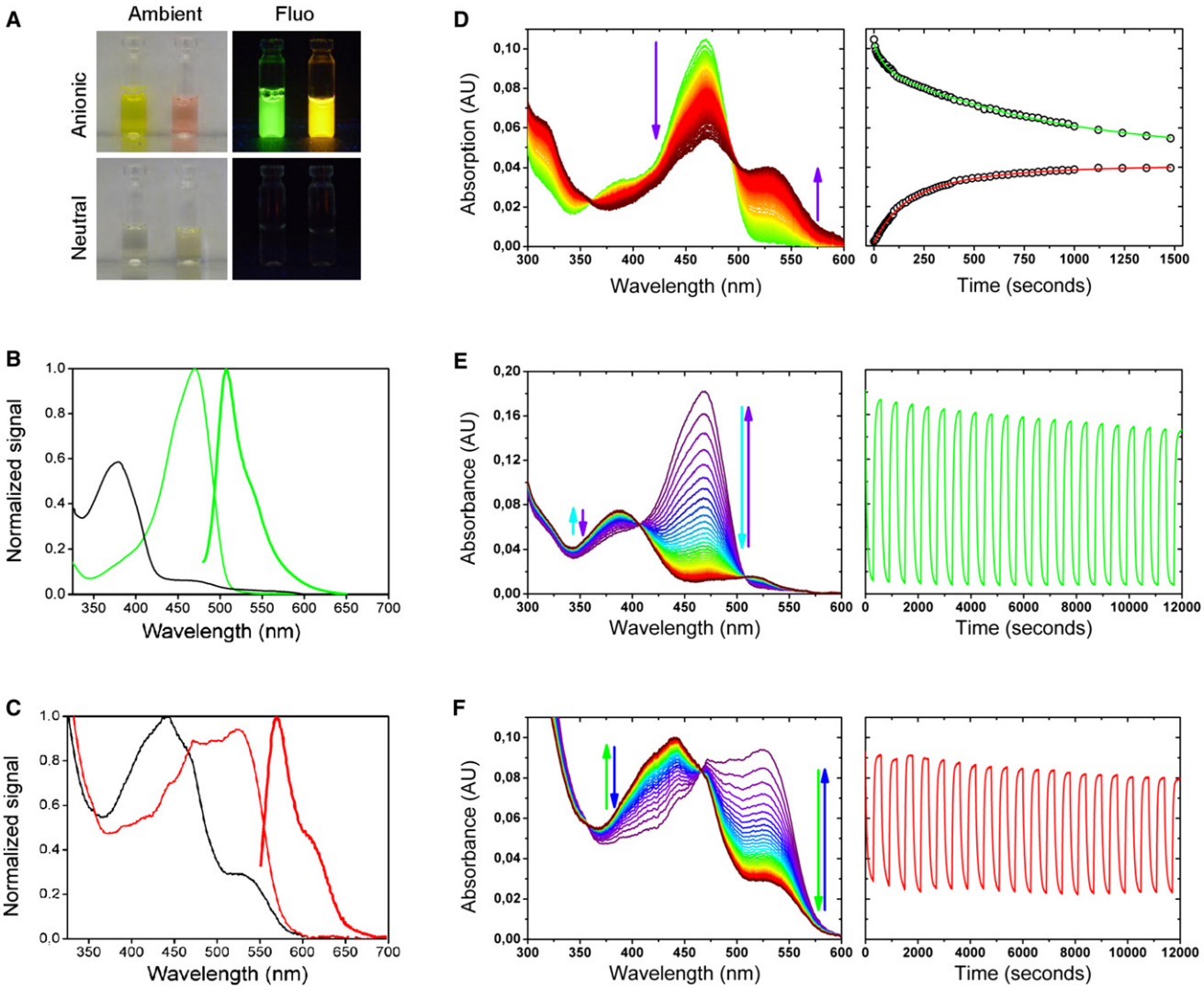

Figure 4. Spectroscopic Properties of NijiFP

(A) Photographs of the nonphotoconverted and photoconverted form NijiFP in its pH-induced anionic and neutral state under ambient and UV light.

(B and C) Absorption (thin lines) and emission (thick lines) spectra of the green form of NijiFP (B) in both the on-state (green) and the off state (black) and of the red form (C) in the on-state (red) and the off state (black).

(D–F) Photoconversion and photochromic behavior of NijiFP. (D) During irradiation with 405-nm light, absorption spectra were acquired and the absorbance at 528 nm, indicative for the red species, was plotted in time. (E) The green species of NijiFP was switched off by 488-nm light and back on by 405-nm light for 20 times and the absorbance at 469 nm was plotted in time. (F) The red species of NijiFP was switched off by 561-nm light and back on with 440-nm light for 20 times and the absorbance at 528 nm was again plotted in time. See also Figure S2 and Figure S3.

colored panels, respectively. We determined the localization precision, by calculating the standard deviation of multiple localizations of the same molecule, to be ~25 nm for the green species and ~35 nm for the photoconverted red species.

SIGNIFICANCE

We have shown that in mEosFP and Dendra2, a single point mutation is sufficient to generate excellent on/off photochromic behavior on top of the existing green-to-red photoconversion. This indicates that these proteins are very prone to switch once their chromophore and/or its microenvironment gains in conformational freedom. Spectroscopic characterization of mEosFP and Dendra2 mutants, the crystal structure of mEosFP and MD simulations provided us with a more precise view on the importance of certain residues in the chromophore environment on photoswitching behavior. As a result of our findings, it is now possible to formulate a lucid summary of the role of key residues in the chromophore environment (Figure 1; Table S1) with respect to their spectroscopic and photochromic importance. Whereas rather bulky residues at positions 159 and 173 inhibit photochromism, smaller residues induce on/off photochromism, accompanied by an increase in Stokes shift due to a blue shifted absorption peak. Mutating the residue at position 157 is not sufficient by itself

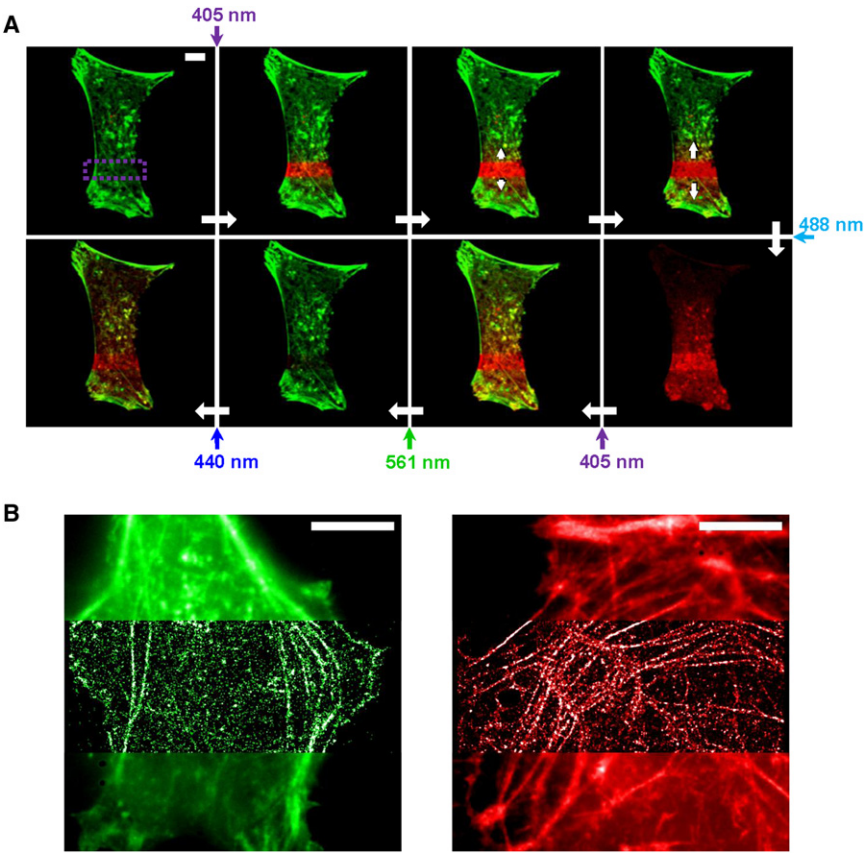

Figure 5. Dynamics and Subdiffraction Structure of Actin Visualized by NijiFP

(A) A living HeLa cell expressing NijiFP-actin was imaged using confocal microscopy with a pixel size of 210 × 210 nm and a pixel dwelling time of 2 μs/pixel. In a specific region of interest (purple rectangle), NijiFP was converted to the red state (300 scans with a 405-nm laser at 526 W/cm^2) and the actin's motion in the cell are easily observable (white arrows). The green and red species could be efficiently switched off (16 scans with a 488-nm laser at 200 W/cm^2 and 50 scans with a 561-nm laser at 500 W/cm^2, respectively) and back on (single scan with a 405-nm laser at 47 W/cm^2 and 40 scans with a 440-nm laser at 260 W/cm^2, respectively). On/off photoswitching and green-to-red photoconversion were induced using a pixel dwelling time of 4 μs/pixel.

(B) Wide-field and PALM images of fixed HeLa cells expressing NijiFP-actin in both the green and photoconverted red forms. Scale bars represent 10 μm. See also Figure S6 and Table S7.

to induce photochromic behavior, but can alter the rates of on- and off-switching. Although the nature of amino acids at positions 157 and 173 seems to have no obvious influence on green-to-red photoconversion, position 159 is of major importance in the photoconversion process. Mutating a polar residue at this position toward a neutral one, results in a decreased efficiency of photoconversion. We introduced NijiFP, a monomeric fluorescent protein that can be very efficiently photoconverted from a green- to a red-emitting species and shows reversible photoswitching behavior in both species. We have shown that NijiFP has superior spectroscopic properties allowing its use as a label in cells for advanced microscopic imaging.

EXPERIMENTAL PROCEDURES

Construction of Mutants and Fusion Proteins

Dendra2, mEosFP, Dronpa and IrisFP were subcloned into a pRSET vector (Invitrogen). Mutations were introduced using a PCR-based technique (Sawano and Miyawaki, 2000). *Escherichia coli* JM109(DE3) cells (Promega, Madison, WI) were transformed for protein expression. Preparation of recombinant proteins and measurements by analytical ultracentrifugation are described elsewhere (Mizuno et al., 2010a). For more details, see Supplemental Information.

For mammalian expression of proteins fused to actin, either mEosFP, mEosFP F173S, Dendra2, or Dendra2 F173S was substituted for Dronpa in Dronpa-β-actin/pMC1 (Mizuno et al., 2010a). HeLa cells on glass bottom dishes (MatTek Corp., Ashland, MA) were transfected using FuGENE6 (Roche Applied Science, Penzberg, Germany) according to the manufacturer's protocol. Cells were fixed with 4% formaldehyde in PBS (Thermo Scientific, Waltham, MA) and subjected to confocal and/or PALM imaging.

Ensemble Spectroscopic Characterization

Absorption spectra were acquired using a Shimadzu UV-1650PC spectrophotometer (Shimadzu Kyoto, Japan). Excitation and emission spectra were acquired using a Fluorolog 3-22 fluorimeter (HORIBA Jobin-Yvon, Longjumeau, France). Absolute quantum yields were measured using an integrating sphere (HORIBA Jobin-Yvon). Measuring extinction coefficients was performed based on Ward's method (Ward, 1981; Ward et al., 1980).

Fluorescence lifetimes were measured using a single photon counting setup that has been described in detail previously (Maus et al., 2001). Excitation wavelengths were 488 nm and 550 nm for green and red forms, respectively. The width of the instrument response function was ~30 ps. Fluorescence decays were globally-fitted using the software FAST (Edinburgh Instruments, Livingston, UK) with a single exponential model or a double exponential model.

Reversible photoswitching and irreversible photoconversion were characterized at the ensemble level using a dedicated home-made setup. Absorption spectra were measured as a function of time using a UV-VIS-NIR light source (DT-MINI-2-GS, Ocean Optics, Duiven, The Netherlands) and a CCD spectrometer (USB4000-UV-VIS, Ocean Optics). The sample was irradiated by different lasers controlled by internal and external shutters. Shutters and acquisition were controlled by home-written software based on Igor Pro (Wave Metrics, Lake Oswego, OR). Data analysis was performed in Igor Pro and Origin (OriginLab, Northampton, MA).

Structural Studies and Numerical Simulations

mEosFP was overexpressed and purified as EosFP (Wiedenmann et al., 2004). Long needle-shaped crystals (0.04 × 0.04 × 0.8 mm^3) were grown at 20°C in 2.2 M ammonium sulfate, 0.1 M Tris/HCl (pH 8.5). Crystals formed after a few days via phase transition from a protein precipitate (Ostwald ripening). X-ray data were collected at 100 K at the European Synchrotron Radiation Facility (ESRF) on beamline ID14-3 (X-ray wavelength λ = 0.931 Å). Data sets were integrated and scaled with XDS (Kabsch, 1993). Data collection and model refinement statistics are compiled in Table S2.

The crystal structure (PDB ID: 3P8U) was solved at 2.25 Å resolution by molecular replacement with Phaser (McCoy et al., 2007), using the coordinates of one monomer of the wild-type EosFP (PDB ID: 1ZUX) as a search model. During the refinement, the two residues Val123 and Thr158 were changed to

Thr and His, respectively, and these mutations appeared very clearly in difference maps residuals. Crystallographic refinement was performed with Refmac (Murshudov et al., 1997) and Coot (Emsley and Cowtan, 2004). Chromophore restraints were generated in Libcheck from idealized coordinates found in the Hic-Up database.

Starting from the crystal structure of mEosFP, we modeled the anionic and neutral forms of the protein and its M159A variant. The pKa of titrable residues were calculated with the H^++ web server (Gordon et al., 2005). We deduced the protonation states for pH values of one unit above and below the experimental pKa of the chromophore for the anionic and neutral forms, respectively. The hydrogen bond network of the protonated models was optimized with structural water molecules, using PDB 2PQR (Dolinsky et al., 2007).

All successive simulations were performed with the fDynamo library (Field et al., 2000). After energy-minimization of the protein in solution, Langevin MD simulations at 300 K were performed within an unfixed region of ~12 Å around the hydroxyl group of the chromophore. After equilibration, each simulation covered 500 ps and structures were saved every 0.1 ps for statistical analysis. Further details on the pKa calculations, selected parameters and atomistic simulations are provided in Supplemental Information.

Microscopy

Confocal fluorescence images were acquired with a laser-scanning microscope (Fluoview FV1000; Olympus, Tokyo, Japan) equipped with 405-, 440-, and 561-nm diode lasers and a 488-nm DPSS laser (Spectra Physics, Irvine, CA). The objective and the excitation dichroic mirror used were UPlan SApo60 × /1.35 and DM405/488/559/635, respectively (Olympus). The image size was adjusted to 512 × 512 pixels, with the pixel size corresponding to ~200 nm. The pixel dwelling time was 4 μs/pixel, and a 4 × Kalman filter was applied to reduce noise in the image. Specimens were alternately scanned with 488-nm (52 W/cm^2) and 561-nm (250 W/cm^2) lasers to sequentially acquire green and red channel images. Fluorescence signals were split into green (500–550 nm) and red (580–680 nm) channels with a SDM560 dichroic mirror (Olympus).

Proteins were photoconverted from green to red by scanning 300 times with the 405-nm laser (526 W/cm^2). For the off-switching of the green state molecules, 16 scans with the 488-nm laser (200 W/cm^2) were applied, whereas the on-switching to the original green state was achieved by a single scan with the 405-nm laser (47 W/cm^2). The off-switching of the molecules in the red state was accomplished by 50 scans with the 561-nm laser (500 W/cm^2), whereas their recovery was induced by scanning 40 times with the 440-nm laser (260 W/cm^2). For details about acquisition, localization and reconstruction resulting in PALM images, see Supplemental Information.

ACCESSION NUMBERS

Coordinates of mEosFP have been deposited in the Protein Data Bank with accession code 3P8U.

SUPPLEMENTAL INFORMATION

Supplemental Information includes seven figures, three tables, and Supplemental Experimental Procedures and can be found with this article online at doi:10.1016/j.chembiol.2011.08.007.

ACKNOWLEDGMENTS

The authors thank Dr. Robert K. Neely and Prof. Mark van der Auweraer for help with analysis, interpretation of the lifetime data and fruitful discussions and Dr. Hiroshi Uji-I and Susana Rocha for help with the microscopy imaging. Financial support of the "Fonds voor Wetenschappelijk Onderzoek FWO" (Grants G.0402.09, G0413.10, G0697.11, G0197.11), the K.U. Leuven Research Fund (GOA 2011/03, Center of Excellence INPAC, CREA2007, "Interdisciplinair Onderzoek" IDO/07/010), the Flemish government (long term structural funding-Methusalem funding CASAS METH/08/04) and the Federal Science Policy of Belgium (IAP-VI/27, Tournesol 2009 project T2009.05) is gratefully acknowledged. V.A. thanks Prof. G. Ulrich Nienhaus for providing mEosFP and Dr. Dominique Bourgeois for his help with the crystallographic structure determination. M.L. thanks Dr. Alexey Onufriev and Dr. Paul Czodrowski for their help in the pKa and PEOE charge calculations, respectively as well as the Wellcome Trust for financial support. V.A., P.D., and C.C.D. acknowledge the "FWO" for a postdoctoral visit fellowship, a postdoctoral grant, and a doctoral grant, respectively.

Received: May 31, 2011
Revised: August 4, 2011
Accepted: August 8, 2011
Published: October 27, 2011

REFERENCES

Abbruzzetti, S., Bizzarri, R., Luin, S., Nifosì, R., Storti, B., Viappiani, C., and Beltram, F. (2010). Photoswitching of E222Q GFP mutants: "concerted" mechanism of chromophore isomerization and protonation. Photochem. Photobiol. Sci. *9*, 1307–1319.

Adam, V., Lelimousin, M., Boehme, S., Desfonds, G., Nienhaus, K., Field, M.J., Wiedenmann, J., McSweeney, S., Nienhaus, G.U., and Bourgeois, D. (2008). Structural characterization of IrisFP, an optical highlighter undergoing multiple photo-induced transformations. Proc. Natl. Acad. Sci. USA *105*, 18343–18348.

Adam, V., Mizuno, H., Grichine, A., Hotta, J., Yamagata, Y., Moeyaert, B., Nienhaus, G.U., Miyawaki, A., Bourgeois, D., and Hofkens, J. (2010). Data storage based on photochromic and photoconvertible fluorescent proteins. J. Biotechnol. *149*, 289–298.

Adam, V., Nienhaus, K., Bourgeois, D., and Nienhaus, G.U. (2009). Structural basis of enhanced photoconversion yield in green fluorescent protein-like protein Dendra2. Biochemistry *48*, 4905–4915.

Ando, R., Mizuno, H., and Miyawaki, A. (2004). Regulated fast nucleocytoplasmic shuttling observed by reversible protein highlighting. Science *306*, 1370–1373.

Ando, R., Flors, C., Mizuno, H., Hofkens, J., and Miyawaki, A. (2007). Highlighted generation of fluorescence signals using simultaneous two-color irradiation on Dronpa mutants. Biophys. J. *92*, L97–L99.

Andresen, M., Stiel, A.C., Trowitzsch, S., Weber, G., Eggeling, C., Wahl, M.C., Hell, S.W., and Jakobs, S. (2007). Structural basis for reversible photoswitching in Dronpa. Proc. Natl. Acad. Sci. USA *104*, 13005–13009.

Andresen, M., Stiel, A.C., Fölling, J., Wenzel, D., Schönle, A., Egner, A., Eggeling, C., Hell, S.W., and Jakobs, S. (2008). Photoswitchable fluorescent proteins enable monochromatic multilabel imaging and dual color fluorescence nanoscopy. Nat. Biotechnol. *26*, 1035–1040.

Annibale, P., Scarselli, M., Kodiyan, A., and Radenovic, A. (2010). Photoactivatable fluorescent protein mEos2 displays repeated photoactivation after a long-lived dark state in the red photoconverted form. J. Phys. Chem. Lett. *1*, 1506–1510.

Betzig, E., Patterson, G.H., Sougrat, R., Lindwasser, O.W., Olenych, S., Bonifacino, J.S., Davidson, M.W., Lippincott-Schwartz, J., and Hess, H.F. (2006). Imaging intracellular fluorescent proteins at nanometer resolution. Science *313*, 1642–1645.

Bizzarri, R., Serresi, M., Cardarelli, F., Abbruzzetti, S., Campanini, B., Viappiani, C., and Beltram, F. (2010). Single amino acid replacement makes Aequorea victoria fluorescent proteins reversibly photoswitchable. J. Am. Chem. Soc. *132*, 85–95.

Chudakov, D.M., Lukyanov, S., and Lukyanov, K.A. (2007). Tracking intracellular protein movements using photoswitchable fluorescent proteins PS-CFP2 and Dendra2. Nat. Protoc. *2*, 2024–2032.

Dedecker, P., Hotta, J., Ando, R., Miyawaki, A., Engelborghs, Y., and Hofkens, J. (2006). Fast and reversible photoswitching of the fluorescent protein Dronpa as evidenced by fluorescence correlation spectroscopy. Biophys. J. *91*, L45–L47.

Dedecker, P., Hotta, J., Flors, C., Sliwa, M., Uji-i, H., Roeffaers, M.B., Ando, R., Mizuno, H., Miyawaki, A., and Hofkens, J. (2007). Subdiffraction imaging through the selective donut-mode depletion of thermally stable

photoswitchable fluorophores: numerical analysis and application to the fluorescent protein Dronpa. J. Am. Chem. Soc. *129*, 16132–16141.

Dolinsky, T.J., Czodrowski, P., Li, H., Nielsen, J.E., Jensen, J.H., Klebe, G., and Baker, N.A. (2007). PDB2PQR: expanding and upgrading automated preparation of biomolecular structures for molecular simulations. Nucleic Acids Res. *35* (*Web Server issue*), W522–W555.

Emsley, P., and Cowtan, K. (2004). Coot: model-building tools for molecular graphics. Acta Crystallogr. D Biol. Crystallogr. *60*, 2126–2132.

Field, M.J., Albe, M., Bret, C., Proust-De Martin, F., and Thomas, A. (2000). The dynamo library for molecular simulations using hybrid quantum mechanical and molecular mechanical potentials. J. Comput. Chem. *21*, 1088–1100.

Flors, C., Hotta, J., Uji-i, H., Dedecker, P., Ando, R., Mizuno, H., Miyawaki, A., and Hofkens, J. (2007). A stroboscopic approach for fast photoactivation-localization microscopy with Dronpa mutants. J. Am. Chem. Soc. *129*, 13970–13977.

Fuchs, J., Böhme, S., Oswald, F., Hedde, P.N., Krause, M., Wiedenmann, J., and Nienhaus, G.U. (2010). A photoactivatable marker protein for pulse-chase imaging with superresolution. Nat. Methods *7*, 627–630.

Gordon, J.C., Myers, J.B., Folta, T., Shoja, V., Heath, L.S., and Onufriev, A. (2005). H++: a server for estimating pKas and adding missing hydrogens to macromolecules. Nucleic Acids Res. *33* (*Web Server issue*), W368–W371.

Gurskaya, N.G., Verkhusha, V.V., Shcheglov, A.S., Staroverov, D.B., Chepurnykh, T.V., Fradkov, A.F., Lukyanov, S., and Lukyanov, K.A. (2006). Engineering of a monomeric green-to-red photoactivatable fluorescent protein induced by blue light. Nat. Biotechnol. *24*, 461–465.

Habuchi, S., Ando, R., Dedecker, P., Verheijen, W., Mizuno, H., Miyawaki, A., and Hofkens, J. (2005). Reversible single-molecule photoswitching in the GFP-like fluorescent protein Dronpa. Proc. Natl. Acad. Sci. USA *102*, 9511–9516.

Habuchi, S., Dedecker, P., Hotta, J., Flors, C., Ando, R., Mizuno, H., Miyawaki, A., and Hofkens, J. (2006). Photo-induced protonation/deprotonation in the GFP-like fluorescent protein Dronpa: mechanism responsible for the reversible photoswitching. Photochem. Photobiol. Sci. *5*, 567–576.

Hayashi, I., Mizuno, H., Tong, K.I., Furuta, T., Tanaka, F., Yoshimura, M., Miyawaki, A., and Ikura, M. (2007). Crystallographic evidence for water-assisted photo-induced peptide cleavage in the stony coral fluorescent protein Kaede. J. Mol. Biol. *372*, 918–926.

Heilemann, M., Dedecker, P., Hofkens, J., and Sauer, M. (2009). Photoswitches: key molecules for subdiffraction-resolution fluorescence imaging and molecular quantification. Laser Photon. Rev. *3*, 180–202.

Heilemann, M., van de Linde, S., Schüttpelz, M., Kasper, R., Seefeldt, B., Mukherjee, A., Tinnefeld, P., and Sauer, M. (2008). Subdiffraction-resolution fluorescence imaging with conventional fluorescent probes. Angew. Chem. Int. Ed. Engl. *47*, 6172–6176.

Hell, S.W. (2007). Far-field optical nanoscopy. Science *316*, 1153–1158.

Henderson, J.N., Ai, H.W., Campbell, R.E., and Remington, S.J. (2007). Structural basis for reversible photobleaching of a green fluorescent protein homologue. Proc. Natl. Acad. Sci. USA *104*, 6672–6677.

Hendrix, J., Flors, C., Dedecker, P., Hofkens, J., and Engelborghs, Y. (2008). Dark states in monomeric red fluorescent proteins studied by fluorescence correlation and single molecule spectroscopy. Biophys. J. *94*, 4103–4113.

Hess, S.T., Girirajan, T.P., and Mason, M.D. (2006). Ultra-high resolution imaging by fluorescence photoactivation localization microscopy. Biophys. J. *91*, 4258–4272.

Hoi, H., Shaner, N.C., Davidson, M.W., Cairo, C.W., Wang, J., and Campbell, R.E. (2010). A monomeric photoconvertible fluorescent protein for imaging of dynamic protein localization. J. Mol. Biol. *401*, 776–791.

Kabsch, W. (1993). Automatic processing of rotation diffraction data from crystals of initially unknown symmetry and cell constants. J. Appl. Crystallogr. *26*, 795–800.

Koestler, S.A., Rottner, K., Lai, F., Block, J., Vinzenz, M., and Small, J.V. (2009). F- and G-actin concentrations in lamellipodia of moving cells. PLoS ONE *4*, e4810.

Lelimousin, M., Adam, V., Nienhaus, G.U., Bourgeois, D., and Field, M.J. (2009a). Photoconversion of the fluorescent protein EosFP: a hybrid potential simulation study reveals intersystem crossings. J. Am. Chem. Soc. *131*, 16814–16823.

Lelimousin, M., Noirclerc-Savoye, M., Lazareno-Saez, C., Paetzold, B., Le Vot, S., Chazal, R., Macheboeuf, P., Field, M.J., Bourgeois, D., and Royant, A. (2009b). Intrinsic dynamics in ECFP and Cerulean control fluorescence quantum yield. Biochemistry *48*, 10038–10046.

Li, X., Chung, L.W., Mizuno, H., Miyawaki, A., and Morokuma, K. (2010). A theoretical study on the nature of on- and off-states of reversibly photoswitching fluorescent protein Dronpa: absorption, emission, protonation, and Raman. J. Phys. Chem. B *114*, 1114–1126.

Lukyanov, K.A., Chudakov, D.M., Lukyanov, S., and Verkhusha, V.V. (2005). Innovation: photoactivatable fluorescent proteins. Nat. Rev. Mol. Cell Biol. *6*, 885–891.

Maus, M., Rousseau, E., Cotlet, M., Schweitzer, G., Hofkens, J., Van der Auweraer, M., De Schryver, F.C., and Krueger, A. (2001). New picosecond laser system for easy tunability over the whole ultraviolet/visible/near infrared wavelength range based on flexible harmonic generation and optical parametric oscillation. Rev. Sci. Instrum. *72*, 36–40.

McCoy, A.J., Grosse-Kunstleve, R.W., Adams, P.D., Winn, M.D., Storoni, L.C., and Read, R.J. (2007). Phaser crystallographic software. J. Appl. Crystallgr. *40*, 658–674.

Millington, M., Grindlay, G.J., Altenbach, K., Neely, R.K., Kolch, W., Bencina, M., Read, N.D., Jones, A.C., Dryden, D.T., and Magennis, S.W. (2007). High-precision FLIM-FRET in fixed and living cells reveals heterogeneity in a simple CFP-YFP fusion protein. Biophys. Chem. *127*, 155–164.

Mizuno, H., Dedecker, P., Ando, R., Fukano, T., Hofkens, J., and Miyawaki, A. (2010a). Higher resolution in localization microscopy by slower switching of a photochromic protein. Photochem. Photobiol. Sci. *9*, 239–248.

Mizuno, H., Mal, T.K., Wälchli, M., Fukano, T., Ikura, M., and Miyawaki, A. (2010b). Molecular basis of photochromism of a fluorescent protein revealed by direct 13C detection under laser illumination. J. Biomol. NMR *48*, 237–246.

Mizuno, H., Mal, T.K., Wälchli, M., Kikuchi, A., Fukano, T., Ando, R., Jeyakanthan, J., Taka, J., Shiro, Y., Ikura, M., and Miyawaki, A. (2008). Light-dependent regulation of structural flexibility in a photochromic fluorescent protein. Proc. Natl. Acad. Sci. USA *105*, 9227–9232.

Moors, S.L.C., Michielssens, S., Flors, C., Dedecker, P., Hofkens, J., and Ceulemans, A. (2008). How is cis-trans isomerization controlled in dronpa mutants? A replica exchange molecular dynamics study. J. Chem. Theory Comput. *4*, 1012–1020.

Murshudov, G.N., Vagin, A.A., and Dodson, E.J. (1997). Refinement of macromolecular structures by the maximum-likelihood method. Acta Crystallogr. D Biol. Crystallogr. *53*, 240–255.

Nienhaus, G.U., Nienhaus, K., Hölzle, A., Ivanchenko, S., Renzi, F., Oswald, F., Wolff, M., Schmitt, F., Röcker, C., Vallone, B., et al. (2006). Photoconvertible fluorescent protein EosFP: biophysical properties and cell biology applications. Photochem. Photobiol. *82*, 351–358.

Piatkevich, K.D., and Verkhusha, V.V. (2010). Advances in engineering of fluorescent proteins and photoactivatable proteins with red emission. Curr. Opin. Chem. Biol. *14*, 23–29.

Rust, M.J., Bates, M., and Zhuang, X. (2006). Sub-diffraction-limit imaging by stochastic optical reconstruction microscopy (STORM). Nat. Methods *3*, 793–795.

Sawano, A., and Miyawaki, A. (2000). Directed evolution of green fluorescent protein by a new versatile PCR strategy for site-directed and semi-random mutagenesis. Nucleic Acids Res. *28*, E78.

Seifert, M.H., Ksiazek, D., Azim, M.K., Smialowski, P., Budisa, N., and Holak, T.A. (2002). Slow exchange in the chromophore of a green fluorescent protein variant. J. Am. Chem. Soc. *124*, 7932–7942.

Shu, X., Shaner, N.C., Yarbrough, C.A., Tsien, R.Y., and Remington, S.J. (2006). Novel chromophores and buried charges control color in mFruits. Biochemistry *45*, 9639–9647.

Stiel, A.C., Trowitzsch, S., Weber, G., Andresen, M., Eggeling, C., Hell, S.W., Jakobs, S., and Wahl, M.C. (2007). 1.8 A bright-state structure of the reversibly

switchable fluorescent protein Dronpa guides the generation of fast switching variants. Biochem. J. *402*, 35–42.

Subach, F.V., Patterson, G.H., Manley, S., Gillette, J.M., Lippincott-Schwartz, J., and Verkhusha, V.V. (2009). Photoactivatable mCherry for high-resolution two-color fluorescence microscopy. Nat. Methods *6*, 153–159.

Subach, F.V., Patterson, G.H., Renz, M., Lippincott-Schwartz, J., and Verkhusha, V.V. (2010). Bright monomeric photoactivatable red fluorescent protein for two-color super-resolution sptPALM of live cells. J. Am. Chem. Soc. *132*, 6481–6491.

Tsutsui, H., Karasawa, S., Shimizu, H., Nukina, N., and Miyawaki, A. (2005). Semi-rational engineering of a coral fluorescent protein into an efficient highlighter. EMBO Rep. *6*, 233–238.

Tsutsui, H., Shimizu, H., Mizuno, H., Nukina, N., Furuta, T., and Miyawaki, A. (2009). The E1 mechanism in photo-induced beta-elimination reactions for green-to-red conversion of fluorescent proteins. Chem. Biol. *16*, 1140–1147.

Voityuk, A.A., Michel-Beyerle, M.E., and Rösch, N. (1998). Quantum chemical modeling of structure and absorption spectra of the chromophore in green fluorescent proteins. Chem. Physiol. *231*, 13–25.

Voliani, V., Bizzarri, R., Nifosì, R., Abbruzzetti, S., Grandi, E., Viappiani, C., and Beltram, F. (2008). Cis-trans photoisomerization of fluorescent-protein chromophores. J. Phys. Chem. B *112*, 10714–10722.

Ward, W.W. (1981). Bioluminescence and Chemiluminescence: Basic Chemistry and Analytical Applications (New York: Academic Press).

Ward, W.W., Cody, C.W., Hart, R.C., and Cormier, M.J. (1980). Spectrophotometric identity of the energy transfer chromophores in Renilla and Aequorea green-fluorescent proteins. Photochem. Photobiol. *31*, 611–615.

Wiedenmann, J., Ivanchenko, S., Oswald, F., Schmitt, F., Röcker, C., Salih, A., Spindler, K.D., and Nienhaus, G.U. (2004). EosFP, a fluorescent marker protein with UV-inducible green-to-red fluorescence conversion. Proc. Natl. Acad. Sci. USA *101*, 15905–15910.